Supplemental Material for ***A Regional Hydrological Model for Arid and Semi-Arid River Basins with Consideration of Irrigation***

Cong Jiang[a,*], Eric J. R. Parteli[b], Qian Xia[c], Xin Yin[a] and Yaping Shao[a]

[a]*Institute for Geophysics and Meteorology, University of Cologne, Pohligstr. 3, Cologne, 50969, North Rhine-Westphalia, Germany*
[b]*Faculty of Physics, University of Duisburg-Essen, Duisburg, Lotharstr. 1, 47057, North Rhine-Westphalia, Germany*
[c]*School of Water Resources and Hydropower Engineering, Wuhan University, Bayi road. 299, 430072, Hubei Province, China*

Abstract: In Sections 1-4 of this Supplemental Material (SM), we provide further information about the hydrological model introduced in Section 2 of the main document. Moreover, in Section 5 of this SM, the impacts of the four most influential reservoirs along Yellow River's mainstream, in the period from 1977 to 1988, are discussed, while the Noah-MP parameterization options used are described in Section 6. The sensitivity analysis of the annual cycles of averaged weekly streamflow on the hydrological parameters, including the parameters β, B, W, n, α and C_s defined in the both main document and SM, is then presented in Section 7. Furthermore, Section 8 provides the spatial distribution of the hydrological variables including (a) precipitation, (b) evapotranspiration, (c) runoff, (d) streamflow, (e) soil moisture, (f) groundwater depth, (g) surface runoff, (h) subsurface runoff, for the Yellow River basin averaged from 1979 to 1988. To conclude this SM, Section 9 presents the calibration and sensitivity analysis of the irrigation model parameters on the irrigation amount and streamflow.

S1. Infiltration and Infiltration-excess runoff

Infiltration capacity or maximum infiltration rate ($I_{\max}$) is a variable that determines the surface water input distribution between infiltration and runoff. The infiltration capacity indicates the infiltration rate under the condition of sufficient water supply, and depends on the characteristics of the soil, such as soil moisture and texture.

Previous studies (Beven, 1989; Chamizo et al., 2012; Gao et al., 2015; Yu et al., 1999) indicated that the soil infiltration capacity is, indeed, much smaller than the saturated hydraulic conductivity at surface ($K_{\mathrm{sat}}(0)$) in a coarse grid, owing to the spatial heterogeneity in hydraulic parameters of

soil and precipitation. We thus assume the following model (Best et al., 2011),

$$I_{\max} = \beta K_{\text{sat}}(0) \tag{S1}$$

$$R_{\text{ins}} = \max(0, Q_{\text{wat}} - I_{\max}) \tag{S2}$$

$$I_{\text{sfc}} = Q_{\text{wat}} - R_{\text{ins}} \tag{S3}$$

where β is an empirical parameter ($0 \leq \beta \leq 1$), which can be determined by calibration of the annual average runoff in the sub-basins of the Yellow River Basin, R_{ins} is the infiltration-excess runoff, Q_{wat} is the water input on the soil surface, and I_{sfc} is the infiltration rate at the surface.

S2. Interaction fluxes of river-groundwater and river-vadose

Given the river channel considered in HMS, the river-groundwater (C_{g}) and river-vadose (C_{u}) interaction fluxes are also computed here using Darcy's law (Sophocleous, 2002; Yu et al., 2006). It is assumed that there is a layer of low-permeability material at the riverbed so that the water in the river can be separated from the groundwater system in each grid. If the water table is higher than the river bed, then C_{g} is proportional to $h_{\text{r}} - h_{\text{g}}$, and $C_{\text{u}} = 0$, where h_{r} is the river water level and h_{g} is the groundwater level. If the groundwater level is lower than the riverbed, then C_{u} is proportional to $h_{\text{r}} - h_{\text{bot}}$, and $C_{\text{g}} = 0$, where h_{bot} is the elevation of the stream bed. The exchange flow between river and groundwater is then calculated using,

$$C_{\text{g}} = \frac{K_{\text{b}}}{M}\left(h_{\text{r}} - h_{\text{g}}\right) = C_{\text{s}}\left(h_{\text{r}} - h_{\text{g}}\right) \tag{S4}$$

$$C_{\text{u}} = C_{\text{s}}(h_{\text{r}} - h_{\text{bed}}) \tag{S5}$$

where C_{s} is the hydraulic conductance of stream-aquifer interconnection [s^{-1}], K_{b} is the hydraulic conductivity of streambed material [m s^{-1}], M is the streambed thickness [m], h_{r} is the stream water level [m], h_{g} is the groundwater head [m], and $h_{\text{bed}}$is the streambed elevation [m]. The hydraulic conductance of the riverbed usually needs to be calibrated against the observed base flow of the river. The sensitivity of AHMS to C_{s} is discussed in Section 7.

S3. Channel bathymetry and floodplain

We assume that the hydraulic geometric shape of the channel follows the power-law function of the bank full discharge Q_{BF} (Leopold & Maddock, 1953), i.e.,

$$w = aQ_{\mathrm{B}}^{b} \tag{S6}$$

$$d = cQ_{\mathrm{BF}}^{f} \tag{S7}$$

where Q_{BF} $[\mathrm{m}^3\mathrm{s}^{-1}]$ is estimated by multiplying the upstream area by the uniform local river input (assuming that the local river input is 0.5 mm/day based on the average of historical data) for each cell (Yu et al. 2006), while the coefficients a and c and the exponents b and f must be determined from observations. According to Parker (1979), the scale factors (a and c) vary over different locations, while the values of the exponents b (~0.5) and f (0.3~0.4) exhibit a remarkable degree of consistency. Here we assume $b = 0.5$ and $f = 0.3$, which are values roughly consistent with the observations of Leopold and Maddock (1953), who estimated the values of these exponents for river basins. Furthermore, we estimate $a = 5.0$ through measurements of the river width from Google Earth satellite imagery, and we assume $c = 0.6$ in consistency with observations of shallow river cross sections throughout the Yellow River Basin. Indeed, the Yellow River has a wide and shallow cross-section throughout the Hetao and North China Plains (China River Sediment Bulletin 2000 for Yangtze River and Yellow River), and is shallow at its lower reaches owing to the flat terrain in the area and the associated strong sediment deposition in the channel. Since the river routing model needs to define the width w and depth d of the channel in each grid, we assume that the minimum values of depth and width are 2 m and 10 m, respectively. The sensitivity of the AHMS to river geometry (width and depth) is discussed in Section 7. The width and depth of the river are defined as follows

$$\begin{cases} w = \max\left[5.0 \cdot Q_{\mathrm{BF}}^{0.5}, 10\right] \\ d = \max[0.6 \cdot Q_{\mathrm{BF}}^{0.3}, 2] \end{cases} \tag{S8}$$

Flood inundation is simulated using the storage model in Cunge (1980) and De Paiva et al. (2013), i.e., assuming that (1) the flow velocity parallel to the river direction vanishes on the floodplain, (2) the floodplain acts only as storage areas, and (3) the water level of the floodplain equals the water level of the main channel. The fractional area of the riverbed f_{b} is then estimated as

$$f_{\mathrm{b}} = \left(\frac{w}{\Delta_x}\right)^{\alpha} \tag{S9}$$

where w is the width of the channel [m] and Δ_x is the grid size [m]. The default value of α is 0.5, which is in general related to the river's meandering and floodplain geometry. However, the sensitivity of AHMS to floodplain geometry is discussed in Section 7.

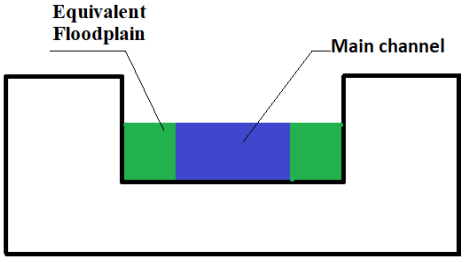

Figure S1: Simple river-floodplain storage model used in the sub-grid cross-section of the AHMS. The main channel area (blue) corresponds to the parameter A_{c} in Eq. (4). Furthermore, the equivalent floodplain area (green) is based on f_{b}, which is computed using Eq. (C.4). Modified after Cunge (1980).

S4. Terrestrial water budget and changes

This section describes the terrestrial water budget equation used in this study. The discharge and balance of water play a key role in the water cycle. Therefore, the quantification and assessment of terrestrial water storage budget and changes constitute an essential prerequisite for the reliable simulation of hydrological processes. The total terrestrial water storage S_{t} and the terrestrial water balance are computed using

$$S_{\mathrm{t}} = W_{\mathrm{sn}} + W_{\mathrm{un}} + W_{\mathrm{sf}} + W_{\mathrm{gw}} \tag{S10}$$

$$\frac{\mathrm{d}S_{\mathrm{t}}}{\mathrm{d}t} = P_{\mathrm{r}} - \mathrm{ET} - R_{\mathrm{sf}} - R_{\mathrm{sub}} \tag{S11}$$

where S_{t} is the total terrestrial water storage [m], W_{sn} is the water storage in snowpack (liquid equivalent) [m], W_{un} is the soil moisture storage in the unsaturated soil layer [m], W_{sf} is the surface water storage [m], including water storage in the rivers, lakes and reservoirs, W_{gw} is the groundwater water storage [m], P_{r} is the precipitation [m s^{-1}], ET is the evapotranspiration [m s^{-1}], R_{sf} is the surface runoff [m s^{-1}], including infiltration-excess runoff and saturation excess runoff, and R_{sub} is the subsurface runoff [m s^{-1}], which includes the interaction fluxes of river-groundwater C_{g} and river-vadose C_{u}.

S5. Major Reservoirs along the Yellow River

Human activities, such as irrigation and dam regulation, play an important role in the Yellow River Basin area. Table S1 shows the information on the four most influential constructed reservoirs along the mainstream of the Yellow River, while Figure S.2 shows the annual cycle of the Longyangxia, Liujiaxia and Sanmenxia Reservoir inflow and outflow. This figure indicates that, during the period from 1979 to 1988, streamflow through Longyangxia and Sanmenxia reservoirs (left and right subfigures in Fig. S.2) was little affected by artificial regulation because of unfinished construction work and reservoir sedimentation. However, streamflow through the Liujiaxia reservoir (subfigure in the centre of Fig. S.2) was greatly affected by artificial regulation. The Liujiaxia Reservoirs increased substantially the baseflow in spring for water supply to the downstream agricultural irrigation areas and decreased streamflow slightly in summer and autumn for flood interception during the period from 1979 to 1988.

Table S1 Information of four major reservoirs along the mainstream of Yellow River

Reservoirs	Location	Height (m)	Storage (10^9 m^3)	Time of completion
Sanmenxia	Middle reaches	335	9.7	September 1960
Liujiaxia	Upper reaches	147	5.7	October 1968
Longyangxia	Upper reaches	178	27.6	October 1986
Xiaolangdi	Middle reaches	160	12.7	October 1999

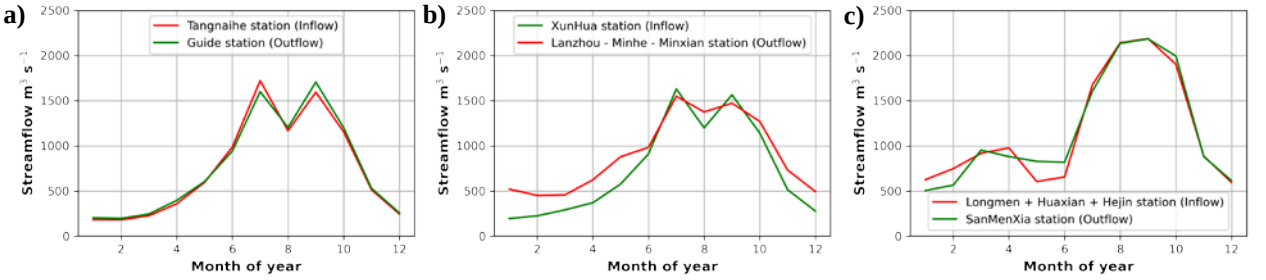

Figure S2: Annual cycles of measured monthly inflow (Tangnaihe station) and outflow (Guide station) of the Longyangxia reservoir (a), monthly inflow (Xunhua station) and outflow (Lanzhou minus Minhe and Minxian station) of the Liujiaxia reservoir (b) and monthly inflow (Longmen plus Haxian and Hejin station) and outflow (Sanmenxia station) of the Sanmenxia reservoir (d), averaged over 1979-1988.

S6. Noah-MP parameterization

Table S2 Noah-MP parameterization options used in this study

Parameterizations Description	**Schemes Used**
Dynamic vegetation	4: table LAI, shdfac = maximum
Stomatal resistance	1: Ball-berry, related to photosynthesis (Ball et al., 1987)
Soil moisture factor controlling stomatal resistance	1: Noah scheme, function of moisture (Chen & Dudhia, 2001)
Runoff and groundwater	9: Darcy's law (Xia, 2019)
Surface exchange coefficient for heat	1: M-O (Brutsaert, 2013)
Supercooled liquid water in frozen soil	NY06 (Niu & Yang, 2006)
Frozen soil permeability	1: NY06 (Niu & Yang, 2006)
Radiation transfer	3: gap = 1—FVEG
Snow surface albedo	2: CLASS (Verseghy, 1991)
Partitioning precipitation into rainfall and snowfall	1: Jordan91 (Jordan, 1991)
Lower boundary condition of soil temperature	1: zero flux
The first-layer snow or soil temperature time scheme	1: semi-implicit

S7. Sensitivity Analysis

Figures S3-S8 display observed annual cycles of averaged weekly streamflow at the main gauging stations along with the associated predictions from our simulations using the different values of β, B, W, n, α and C_s, respectively. As can be seen from these figures, the model results are particularly sensitive to α, β and n. We thus calibrate AHMS to obtain the optimal combination of the two most sensitive river routing parameters (α and n) and soil parameters (β and C_s) for the upper and middle reaches of the Yellow River.

As described in Table S3, the calibrated values of soil saturated hydraulic conductivity amount to $0.028K_{\mathrm{sat}}$, $0.035K_{\mathrm{sat}}$, $0.15K_{\mathrm{sat}}$, and $0.12K_{\mathrm{sat}}$ in the subbasins TNH, TNH-LZ, LZ-TDG, and TDG-HYK, respectively.

Table S3 Experimental design for hydrological parameters sensitivity analysis

Symbol	Name	Unit	Model default	Value
Soil Parameters				
β	Decay factor of soil saturated hydraulic conductivity	-	calibrated in subbasins as 0.028, 0.035, 0.15 and 0.12 × K_{sat}	× 0.5, 1.0, 1.5
C_s	hydraulic conductance of stream-aquifer interconnection	s^{-1}	calibrated in subbasins as 10^{-7}, 10^{-6}, 10^{-6} and 10^{-6}	× 0.1, 1.0, 10
River routing parameters				
w	Channel width	m	$5.0\,Q_{BF}^{0.5}$	× 0.5, 1.0, 1.5
d	Channel depth	m	$0.6\,Q_{BF}^{0.3}$	× 0.5, 1.0,

				1.5
n	Manning roughness coefficient	s $m^{-1/3}$	calibrated in subbasins as 0.025, 0.025, 0.01, 0.01	× 0.5, 1.0, 1.5
α	an exponent used to calculate the fraction of the riverbed	-	0.5	0.4, 0.5, 0.8

Furthermore, in large-scale hydrological simulations, empirical equations are used to estimate channel parameters due to the lack of a large-scale river hydraulic geometry dataset. Indeed, the quantitative assessment of these parameters experienced an improvement in recent years through the progress achieved in advanced satellite data applications. Neal et al. (2012) used high-resolution satellite imagery to estimate the width of rivers, and Yamazaki et al. (2011) developed the Global Width Database of Large Rivers (GWD-LR) based on observed water bodies. Notwithstanding this significant progress, there is still considerably sparsity in the data available for obtaining channel depth and the Manning roughness coefficient in hydrological simulations. Therefore, based on previous research on large-scale river dynamics (De Paiva et al., 2013; Neal et al., 2012; Yamazaki et al., 2011; Yu et al., 2006), the Manning roughness coefficient (n), the coefficients of the hydraulic geometry (B and W), and the exponent of river bed fraction f_b are selected for the sensitivity analysis. The selected model parameters are summarized in Table S3. In particular, the sensitivity analysis consists of perturbing the value of each parameter of the flow routing model in the Yellow River Basin by the factors 0.5, 0 and -0.5.

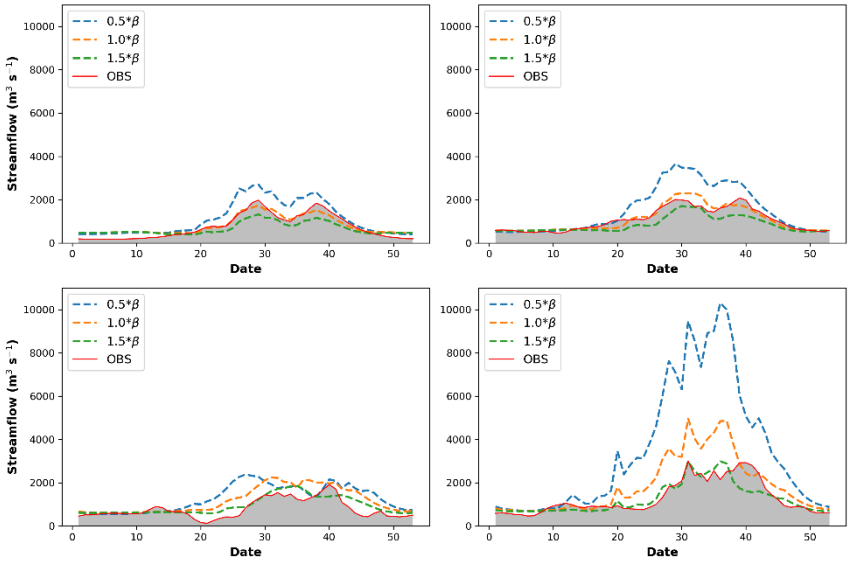

Figure S3: Annual cycles of averaged weekly streamflow for the period of 1979-1988 at six main hydrological stations of the Yellow River, TangnaiHe (a), Lanzhou (b), Toudaoguai (c) and Huayuankou (e), with standard infiltration scheme 0.5β (blue dashed line), 1.0β (orange dashed line), 1.5β (green dashed line) and observed discharge (red solid line with a grey fill), where β is the decay factor of soil saturated hydraulic conductivity.

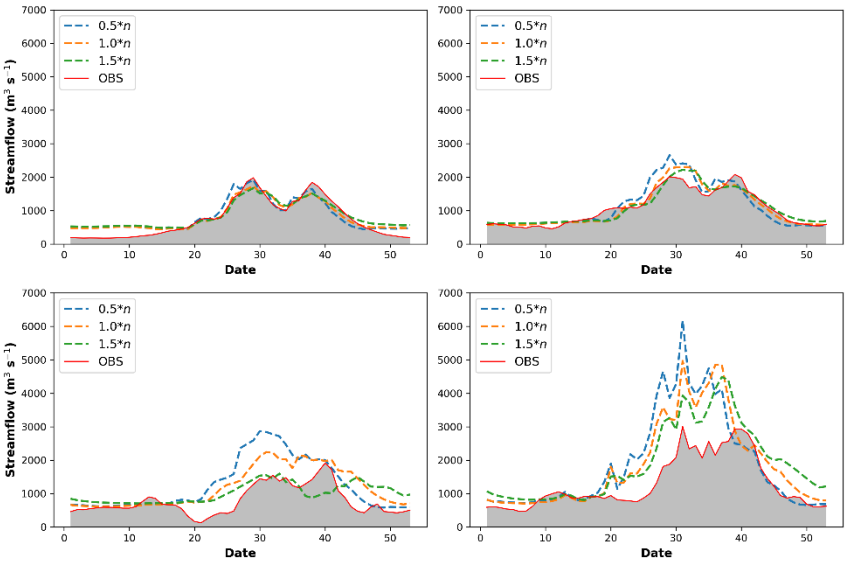

Figure S4: Annual cycles of averaged weekly streamflow for the period of 1979-1988 at four main stations of Yellow River, Tangnaihe (a), Lanzhou (b), Toudaoguai (c) and Huayuankou (d), with Manning roughness coefficient of river $n \times 0.5$ (blue), n (orange), $n \times 1.5$ (green), observed discharge (red solid line with a grey fill).

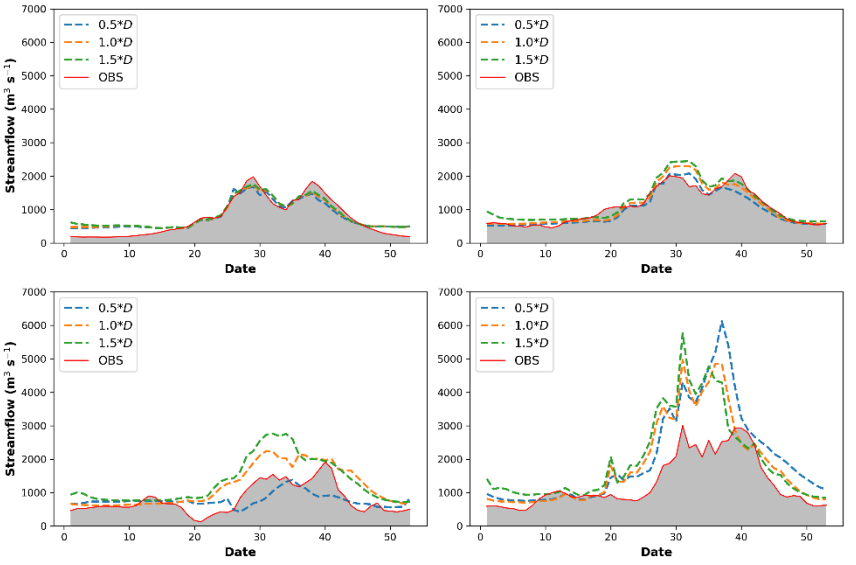

Figure S5: Annual cycles of averaged weekly streamflow for the period of 1979-1988 at four main stations of the Yellow River, Tangnaihe (a), Lanzhou (b), Toudaoguai (c) and Huayuankou (d), with the depth of river $B \times 0.5$ (blue), B (orange), $B \times 1.5$ (green), observed discharge (red solid line with a grey fill).

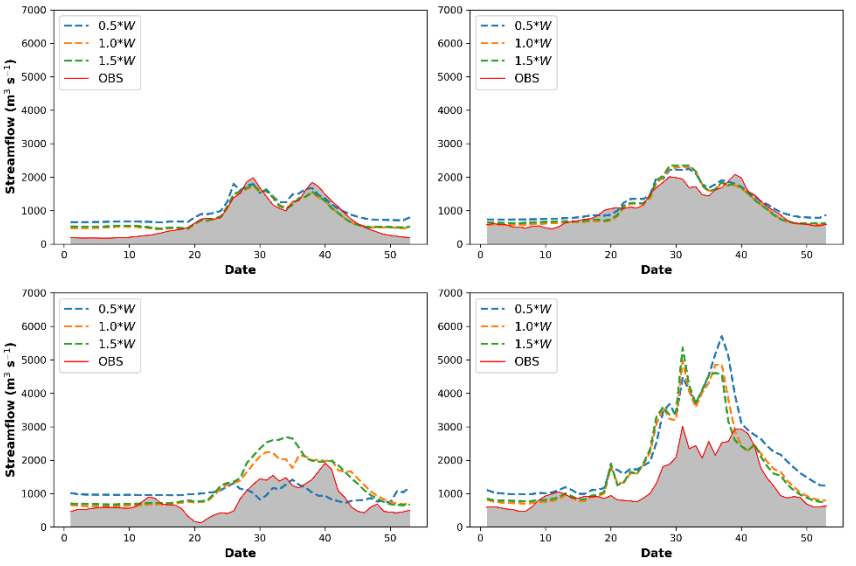

Figure S6: Annual cycles of averaged weekly streamflow for the period of 1979-1988 at four main stations of Yellow River, Tangnaihe (a), Lanzhou (b), Toudaoguai (c) and Huayuankou (d), with the width of the river $W \times 0.5$ (blue), W (orange), $W \times 1.5$ (green), observed discharge (red solid line with a grey fill).

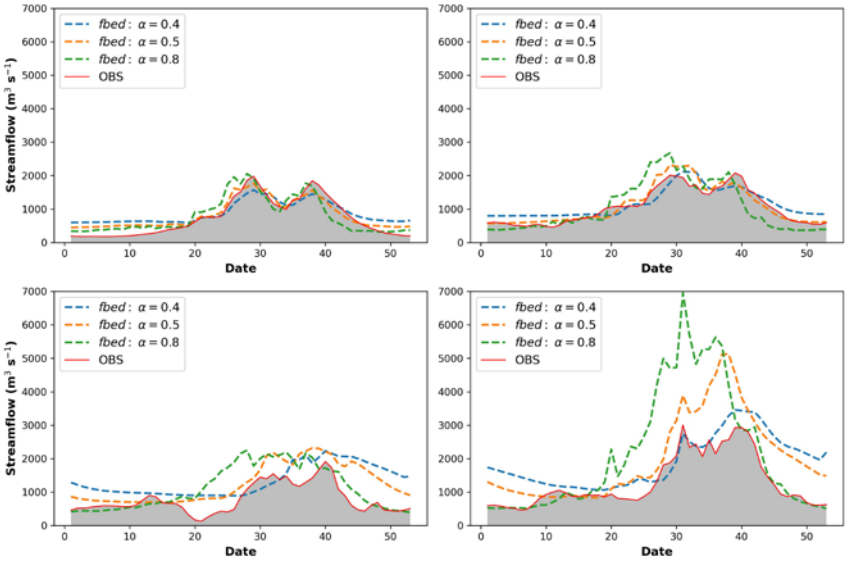

Figure S7: Annual cycles of averaged weekly streamflow for the period of 1979-1988 at four main stations of the Yellow River, Tangnaihe (a), Lanzhou (b), Toudaoguai (c) and Huayuankou (d), with an exponent of the fraction of riverbed α =0.4 (blue), 0.5 (orange), 0.8 (green), observed discharge (red solid line with a grey fill).

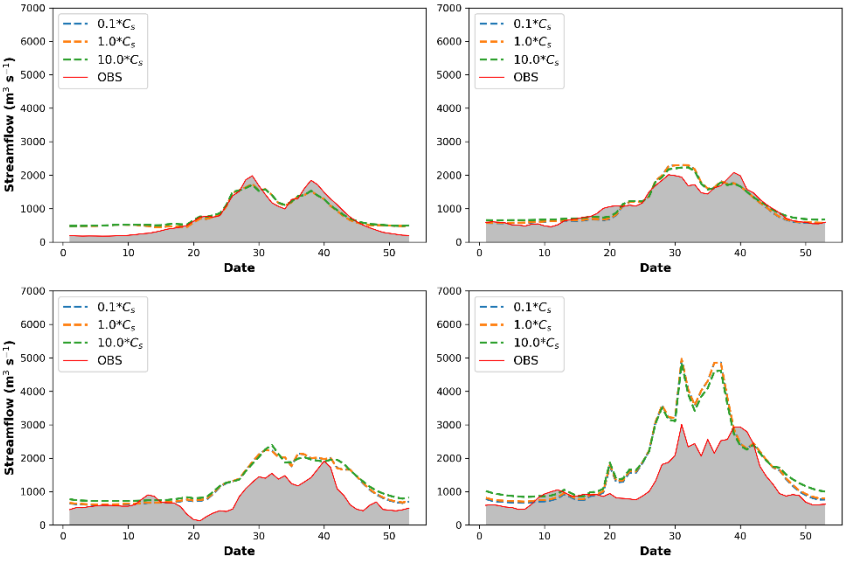

Figure S8: Annual cycles of averaged weekly streamflow for the period of 1979-1988 at four main stations of the Yellow River, Tangnaihe (a), Lanzhou (b), Toudaoguai (c) and Huayuankou (d), with hydraulic conductance of stream-aquifer interconnection C_s =0.4 (blue), 0.5 (orange), 0.8 (green), observed discharge (red solid line with a grey fill).

S8. Spatial Distribution of the Hydrological Variables

Figure S9 shows the spatial distribution of hydrological variables including (a) precipitation, (b) evapotranspiration, (c) runoff, (d) streamflow, (e) soil moisture, (f) groundwater depth, (g) surface runoff and (h) subsurface runoff in the Yellow River Basin, averaged annually from 1979 to 1988. As shown in Fig. S9.a, the Yellow River Basin has a very uneven distribution of precipitation. In particular, this precipitation decreases considerably from south (700-1000 mm/yr) to north (100-200 mm/yr). Moreover, the precipitation distribution correlates strongly with the evapotranspiration map (Fig.S9.b), and appears consistent with the occurrence of two major runoff areas in the southern part of the Yellow River Basin, i.e., the upper reaches and the Wei He River Basin (Fig. S9.c). Furthermore, it can be seen in Fig. S9.d that the river network and flow magnitude predicted by the model match the corresponding observations. Figure S9.e shows that the maximum and minimum values of soil moisture are in the upper reaches and in the arid to semi-arid middle reaches of Yellow River Basin, respectively, and that the spatial distribution of soil moisture follows closely the river network. Moreover, groundwater depth exceeds 25 m over most of the Yellow River Basin (Fig. S9.f), except for the main river networks and the lower reaches – which have groundwater levels under 10 m. Figure S9.g shows that the distributions of runoff and surface runoff are consistent with each other, while it can be seen from Fig. S9.h that subsurface runoff is mainly generated in the upper

reaches, with the Yellow River recharging groundwater from Lanzhou to Toudaoguai.

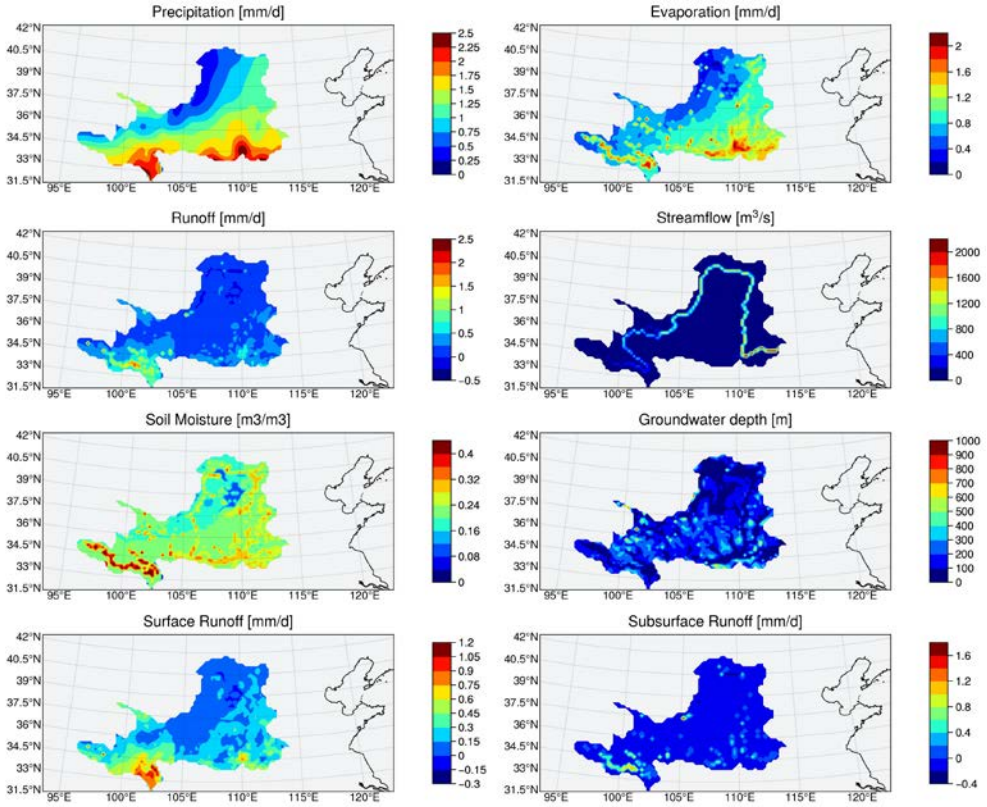

Figure S9: Spatial distribution of mean annual (a) precipitation, (b) evapotranspiration, (c) runoff, (d) streamflow, (e) soil moisture, (f) groundwater depth, (g) surface runoff, (h) subsurface runoff, averaged over 1979-1988, at the Yellow River Basin.

S9. Calibration and sensitivity analysis of irrigation model parameters

Table S4 Experimental design for calibration and validation of irrigation model

Experiment name	Irrigation scheme	Irrigation parameters	Objective
NO_IRR	No	No	As a reference with the calibrated hydrological parameters at the basin scale
CNTL_IRR	Yes	IRR_FRAC=0.25, IR_RAIN= 1.00, IRR_MAD=0.5, IRR_LAI=0.6, FILOSS=0.1	As a reference with the calibrated hydrological and irrigation parameters at the basin scale
MAD_0.4	Yes	Same as CNTL_IRR, but with IRR_MAD=0.4	To test the model sensitivity to IRR_MAD
MAD_0.6	Yes	Same as CNTL_IRR, but with IRR_MAD=0.6	
LAI_0.8	Yes	Same as CNTL_IRR, but with IRR_LAI=0.8	To test the model sensitivity to IRR_LAI
LAI_1.0	Yes	Same as CNTL_IRR, but with IRR_LAI=1.0	

ONLY STRAM	Yes, but sink term $Q_{\mathrm{irr\_sf}}$ in flow routing model only irrigate the main streams flow across cells	Same as CNTL_IRR	As a reference with only irrigating the grid cells the streams flow across

Table S5 Comparison of statistical and simulated areal average annual irrigation in the Yellow River Basin, as well as the NSE of monthly streamflow at outlet of YRB (HYK) from 1979 to 1987 (mm/yr)

Experiment	River irrigation			Groundwater irrigation			Total irrigation			NSE
	Statistics	Sim	PE (%)	Statistics	Sim	PE (%)	Statistics	Sim	PE (%)	
CNTL_IRR	20.45	14.89	-27.19	8.29	11.16	34.98	28.74	26.05	**-9.36**	**0.55**
MAD_0.4		9.89	-51.64		6.66	-7.49		16.55	-42.41	0.53
MAD_0.6		22.66	10.81		19.99	141.13		42.65	48.40	0.50
LAI_0.8		14.39	-29.63		9.60	15.80		23.99	-16.53	0.52
LAI_1.0		13.70	-33.00		9.45	14.00		23.15	-19.45	0.53
ONLY STRAM		**1.81**	-91.15		10.55	27.26		12.36	-57.00	**0.35**

References

Best, M. J., Pryor, M., Clark, D. B., Rooney, G. G., Essery, R., Ménard, C. B., Edwards, J. M., Hendry, M. A., Porson, A., Gedney, N., & others. (2011). The Joint UK Land Environment Simulator (JULES), model description--Part 1: energy and water fluxes. *Geoscientific Model Development*, *4*(3), 677–699.

Beven, K. (1989). Changing ideas in hydrology—the case of physically-based models. *Journal of Hydrology*, *105*(1–2), 157–172.

Chamizo, S., Canton, Y., Lázaro, R., Solé-Benet, A., & Domingo, F. (2012). Crust composition and disturbance drive infiltration through biological soil crusts in semiarid ecosystems. *Ecosystems*, *15*(1), 148–161.

Cunge, J. (1980). Practical aspects of computational river hydraulics. *Pitman Publishing Ltd. London,(17 CUN), 1980*, *420*.

De Paiva, R. C. D., Buarque, D. C., Collischonn, W., Bonnet, M.-P., Frappart, F., Calmant, S., & Bulhões Mendes, C. A. (2013). Large-scale hydrologic and hydrodynamic modeling of the Amazon River Basin. *Water Resources Research*, *49*(3), 1226–1243.

Gao, Y., Li, K., Chen, F., Jiang, Y., & Lu, C. (2015). Assessing and improving Noah-MP land model simulations for the central Tibetan Plateau. *Journal of Geophysical Research: Atmospheres*, *120*(18), 9258–9278.

Leopold, L. B., & Maddock, T. (1953). *The hydraulic geometry of stream channels and some physiographic implications* (Vol. 252). US Government Printing Office.

Neal, J., Schumann, G., & Bates, P. (2012). A subgrid channel model for simulating river hydraulics and floodplain inundation over large and data sparse areas. *Water Resources Research*, *48*(11).

Parker, G. (1979). Hydraulic geometry of active gravel rivers. *Journal of the Hydraulics Division*, *105*(9), 1185–1201.

Sophocleous, M. (2002). Interactions between groundwater and surface water: the state of the science. *Hydrogeology Journal*, *10*(1), 52–67.

Yamazaki, D., Kanae, S., Kim, H., & Oki, T. (2011). A physically based description of floodplain

inundation dynamics in a global river routing model. *Water Resources Research*, *47*(4).

Yu, Z., Lakhtakia, M. N., & Barron, E. J. (1999). Modeling the river-basin response to single-storm events simulated by a mesoscale meteorological model at various resolutions. *Journal of Geophysical Research Atmospheres*, *104*(D16), 19675–19689. https://doi.org/10.1029/1999JD900339

Yu, Z., Pollard, D., & Cheng, L. (2006). On continental-scale hydrologic simulations with a coupled hydrologic model. *Journal of Hydrology*, *331*(1–2), 110–124.